Identification and Analysis of Anomalous Ground Movements in Urban and Rural Areas Using Persistent Scatterer Interferometry in Southern Hesse, Germany

Michael Rudolf, Katrin Krzepek, Benjamin Homuth, Andreas Henk, and Dorota Iwaszczuk

***Abstract*—Thanks to the open publication in recent years, the general public can now view and evaluate ground motion data. However, the data offered in web portals are often only optimized for display, and there is no automatic detection of hotspots and their analysis. In this study, ground motion patterns are investigated using persistent scatterer interferometry data from the Ground Motion Service Germany. We focus on the identification of regions with significant ground motion in cities using a ground motion analyzer, time series analysis, and external data. A case study in Frankfurt am Main shows significant subsidence in the city presumably due to groundwater extraction during the construction phase of various buildings. Another case study in Crumstadt in the northern Upper Rhine Graben reveals pronounced seasonal fluctuations, probably due to factors, such as temperature and activity in a nearby underground storage facility. We show that it is important to include external data, such as temperature, precipitation, and gas storage levels in order to comprehensively analyze the causes of ground movements. Our results contribute to understanding and mitigating the effects of ground motion and highlight the need to analyze time-varying motion in addition to linear velocities.**

***Index Terms*—Ground motion service, time series, urban subsidence, visualization.**

I. Introduction

In MANY regions around the world, anthropogenic and natural processes lead to uplift and subsidence of the Earth's surface. Slow ground movements, caused for example by slope instabilities, tectonic movements, groundwater dynamics, mining activity, and reservoir depletion are difficult to detect and usually only cause visible damage over several decades. In addition, the risk of ground movement is changing in many regions due to the challenges posed by climate change [1], [2]. Slopes that have been stable for a long time can start to move due to thawing permafrost or more frequent heavy rainfall events. Prolonged dry phases and the associated drop in the groundwater level or soil moisture lead to shrinkage of swelling rocks or soils, such as in Offenbach (Hesse, Germany). One consequence of this could be damage to buildings due to irregular or unforeseen ground subsidence. For climate-resilient urban planning, it therefore makes sense to identify risk areas and take countermeasures [3]. The analysis of previous ground movements in a region can help to estimate future behavior.

Ground motion can be determined using remote sensing methods over large areas and longer periods of time. Using the remote sensing technique of differential synthetic aperture radar interferometry (DInSAR) it is possible to measure ground movements in the millimetre range with a spatial resolution of a few metres [4], [5]. Persistent scatterer interferometry (PSI) is a special form of DInSAR [6]. This method uses a long time series and scatterers that persist during the entire time interval of the image acquisition. Depending on the data used, the temporal resolution is only a few days. The scatterers can be either purpose-built corner reflectors or locations that naturally act as corner reflectors, such as the right angle between buildings and roads. Consequently, the density of persistent scatterers (PS) is significantly higher in urban areas than in rural and natural areas. DInSAR and PSI is used to determine groundwater extraction in arid regions (e.g., [7], [8], [9]), mining (e.g., [10], [11]), hydrocarbon extraction (e.g., [12], [13], [14]), or infrastructure monitoring (e.g., [15], [16], [17]). In an increasing number of countries, automated detection of all ground movements is being carried out due to the improvement and easy availability of InSAR products [18], [19], [20].

In this study, we use a two-stage workflow (Fig. 1). In a first step, regions with higher than average vertical movements are highlighted using the ground motion analyzer (GMA) [21]. In principle, this step is similar to ADAfinder [22], [23], [24], but without the cross-correlation between the individual PS. Subsequently, the anomalies found are examined in more detail using inversion-based time series analysis. In addition to linear and sinusoidal (seasonal) signals, this inversion can also be

Manuscript received 27 December 2023; revised 1 March 2024 and 17 April 2024; accepted 26 April 2024. Date of publication 15 May 2024; date of current version 14 June 2024. This work was supported by the Umwelt 4.0 project, Cluster I "Nutzung digitaler Geländemodelle und Copernicus-Daten," the Hessian Ministry for Digital Strategy and Development and coordinated by the Hessian Agency for Nature Conservation, Environment and Geology. *(Corresponding author: Michael Rudolf.)*

Michael Rudolf and Andreas Henk are with the Engineering Geology, Technical University of Darmstadt, 64289 Darmstadt, Germany (e-mail: rudolf@geo.tu-darmstadt.de).

Katrin Krzepek and Dorota Iwaszczuk are with the Remote Sensing and Image Analysis, Technical University of Darmstadt, 64289 Darmstadt, Germany.

Benjamin Homuth is with the Hessian Agency for Nature Conservation, Environment and Geology, 65203 Wiesbaden, Germany.

Digital Object Identifier 10.1109/JSTARS.2024.3400698

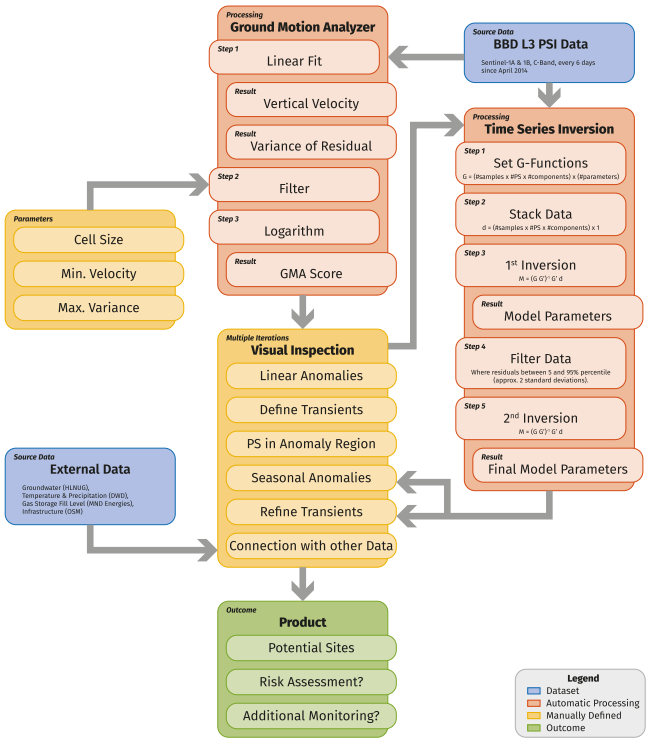

Fig. 1. Workflow used in this study. Using PSI vertical and E-W datasets from the BBD, we compute a ground motion score based on average vertical velocity, filtered by velocity and variance thresholds. After visual inspection, deformation regions are chosen for in-depth analysis using time series methods, detecting seasonal anomalies and transients. The inversion-inspection part is repeated several times to find all relevant transients. The resulting product aids regulatory authorities in risk analysis and preventive measure design.

used to detect transient signals, e.g., caused by water extraction, construction activities and agriculture, or earthquakes, which occasionally occur with small to medium magnitudes in southern Hesse. Both algorithms are available in the open source software package u4py, which was developed as part of the overarching project Umwelt 4.0 (https://git-ce.rwth-aachen.de/rudolf/u4py). Other studies use a similar workflow with subsequent principal component and independent component analysis for understanding slow deformation triggered by rainfall [25]. Some studies use wavelet-based methods to quantify the frequency content and the cross-correlation between PSI and external data, e.g., for groundwater subsidence [26] or seasonal reactivation of landslides [27], [28], while other studies only use qualitative comparisons with the mining activity [10].

The federal state of Hesse in central Germany is also affected by potentially damaging ground movements. Especially in the north of Hesse there are former lignite mines and currently still active salt mining, which leads to frequent landslides in the former and subsidence in the latter. Large areas of the state are covered with landslide-prone geological units and could potentially be areas with increased movement potential [29]. Within the scope of our study, previously unknown ground movements in urban regions are to be detected and then analyzed. Since there are currently no statewide studies on the expected magnitudes and characteristics of the signals of ground movements in PSI data in Hesse, we choose the two-stage procedure outlined above (Fig. 1). Existing methods often necessitate precise prior knowledge of expected movements or are limited to small-scale, regional analyses, particularly in cases where anomalies are hydraulically interconnected. Subsequently, we illustrate our methodology using two distinct regions in south Hesse that are experiencing significant ground movements. We identify and analyze various external factors that might contribute to these phenomena. Further steps will then be taken to draw conclusions about the associated risks and future developments.

II. Methodology

A. Data Preparation

The Ground Motion Service Germany[1] (BBD), which is under the management of the Federal Institute for Geosciences and Natural Resources (BGR) and is a component of the Copernicus Land Monitoring Service, was created using the PSI method and data from the Sentinel-1 satellites. The BBD[2] WebGIS (Web Geographic Information System) application allows the visualization and free download of ground motions. More than 50 million data points with time series spanning from 2015 to December 2021 are included in the dataset [30]. In 2022, the European Environment Agency launched the European Ground Motion Service (EGMS),[3] which covers the majority of Europe. The preprocessing of the BBD data can be found in [30] and is briefly explained in our earlier work [21]. BBD and EGMS are two very powerful institutions that provide validated ground motion information from Europe to stakeholders regardless of their expertise and resources without any processing effort.

Each time one of the two Sentinel-1 twin satellites passes overhead, usually every six days, the phase shift of the radar signal is measured, and a relative shift of the persistent scatterer is derived [6]. These relative motions are shown in the time series as relative displacement. The time series of only one PS can be displayed in the WebGIS applications. At the time of writing, averaged time series of several PS can be visualized in the EGMS, but not in the BBD. There are currently no functions available in the WebGIS application for further analysis of the data (e.g., intersection with other data sets, such as groundwater levels, which can lead to seasonal ground motion). The aim of our work is therefore to present a workflow that makes it possible to visualize PS time series of a region, to derive trends, periodicity and to intersect them with external data.

In this study, we use the PSI dataset of the BBD, published by the BGR, in the area of the federal state of Hesse (state outlined in red in insert of Fig. 2). We focus on two smaller subregions where higher than average linear and seasonal ground motion was detected to illustrate the workflow (blue and orange rectangles in Fig. 2). The analyses use the already separated vertical and horizontal components (L3 data) with a spatial resolution of 50×50 m^2 and a time interval of six days. Each individual data point consists of several PSs which were combined. In addition to the time series, mean values and the variance of the mean

[1]German: Bodenbewegungsdienst Deutschland
[2]accessible at https://bodenbewegungsdienst.bgr.de/
[3]accessible at https://egms.land.copernicus.eu/

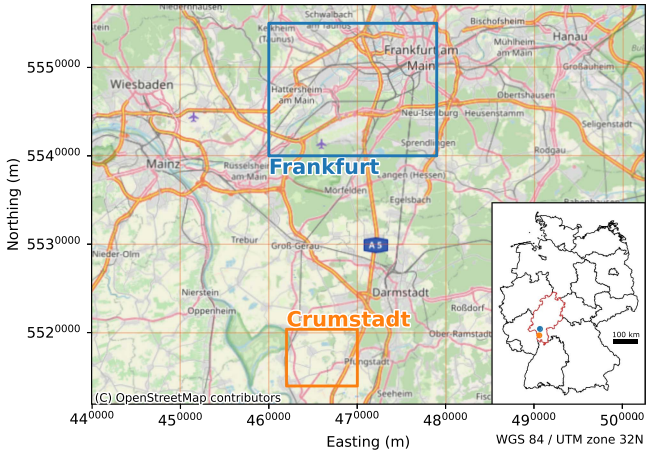

Fig. 2. Regional overview map showing the location of the case study areas in the south of Hesse, Germany. The blue rectangle corresponds to Fig. 4(a) and the orange rectangle to Fig. 5(a). The entire area investigated with the GMA is highlighted in red on the map of Germany.

value are also available. Further information on preprocessing can be found in [30].

B. Ground Motion Analyzer

In this study, we use a custom-built GMA [21] and time series analysis to determine regions of strong ground motion in cities and under infrastructure from the BBD data. At the time of writing, there is no hot-spot detection built into the WebGIS applications to filter the data to focus on areas of strong ground motion. Therefore, we use the variance-based GMA which allows us to visualize regions with strong movement at different spatial scales. These regions are then further investigated with detailed time series analysis, allowing us to identify long-term and short-term components of ground motion. It is already possible to see the average annual ground movement using the visualization in the web portals. However, transient and periodic events are filtered out or distorted by the averaging. Although individual time series can be compared manually, large-scale analyses and statements about seasonal influences are only possible to a limited extent. We therefore combine the GMA with an inversion of the time series in order to extract the individual components and transient events from the available data.

With the GMA, the PSs in an area are filtered based on their variance and the number of PSs. If many PSs show a strong uplift or subsidence, this is highlighted in the respective area. To get the ground motion hotspots first the area is subdivided into cells of a specific cell size. This can be flexibly selected to detect the ground movement on different scales and was set to 250×250 m^2. In each of the cells all PSs that are below a minimum absolute velocity $v_{\min}$ and above a maximum variance $\sigma^2_{\max}$ are removed, which was set to $v_{\min} = 1.5\,\frac{mm}{a}$ and $\sigma^2_{\max} = 1$ in this study. This represents the error range of the available PSI data. Then, the number of remaining PSs in each cell is multiplied by the sum of their velocity. This result is logarithmized which yields a "ground motion score" for each cell. Ground motion hotspots are characterized by scores ≥-1 and are displayed as the output of the GMA.

C. Time Series Analysis

Regions of interest are analyzed using a time series inversion scheme based on an algorithm developed for GNSS measurements [31], [32]. For this we assume that the ground motion d measured at the PS is a linear combination of several components in the form of Green's functions G and model parameters m

$$d = G \cdot m. \tag{1}$$

Inverting for the model parameters m gives

$$m = (G' \cdot G)^{-1} \cdot G' d. \tag{2}$$

Each component can be associated with one or more possible causes of ground motion (Table I). The linear component is associated with long-term deformation that acts over the whole time series, such as tectonic subsidence. Annual or semiannual trends are detected using sinusoidal functions. These describe the changes due to seasonal variation of average temperature or ground water level. Transient events of variable cause are fit with a logistic growth function. It is scaled with the factor k so that the start t_s and end t_e of the transient can be predefined and the point of maximum growth t_0 divides the transient in two equal halves. There is also the option to add other models to the inversion, such as earthquakes including postseismic relaxation. After the inversion, the model parameters show the respective contribution of each component to the measured ground motion. The residuals are analyzed for possible remaining contributions to be implemented in the inversion scheme.

For studying the ground motion patterns, we utilize all PS points in a given region of interest and invert the vertical and horizontal components simultaneously. This yields better and more robust results because single PS are very noisy in some cases. If the visual inspection of the time series indicates that there are one or more transients, this is taken into account accordingly in the parameterization of the Green's functions G. This means that the magnitude of the transient deformation is fitted in a defined range of the time series in the same model in addition to the linear and sinusoidal components. In addition, after a first inversion step we remove all outliers that are outside a 2σ range of the residuals. The second inversion step usually delivers a more accurate result. However, in some cases the residuals are not normally distributed. This is particularly evident when two or more different trends are present in a region of interest. In such cases, the region of interest must be adjusted accordingly so that there are no overlapping trends in the time series.

The analysis of the movements focuses on the vertical component. The horizontal movements in our study area are an order of magnitude smaller than the vertical movements. In addition, differential vertical movements below a building are usually responsible for building damage in the lowlands. Only on steep slopes could the horizontal component play a role, e.g., in the case of solifluction. All of our areas are located in relatively flat areas, which means that we can rule out slope movements. In

TABLE I
COMPONENTS THAT ARE INCLUDED IN THE INVERSION OF THE TIME SERIES

Component	Function
Polynomial: Linear (e.g., tectonic subsidence) and higher order	$[A_1 + A_2 \cdot (t - t_R) + A_3 \cdot (t - t_R)^2 + A_n \cdot (t - t_R)^{n-1} + \dots]$ with t_R as a reference time
Sinusoidal: Annual and semiannual cyclic processes (e.g., temperature, rainfall)	$[B_1 \cdot sin(2\pi t) + B_2 \cdot cos(2\pi t) + B_3 \cdot sin(4\pi t) + B_4 \cdot cos(4\pi t)]$ with max. amplitude $a = \sqrt{B_1^2 + B_2^2 + 2B_1 \cdot (-B_2)\, cos(\varphi_2 - \varphi_1)}$ and peak time $\varphi_0 = tan^{-1}\left(\frac{B_1\, sin\varphi_1 - B_2\, sin\varphi_2}{B_1\, cos\varphi_1 - B_2\, cos\varphi_2}\right)$
Logistic: Transients (e.g., water extraction)	$\left[F_n \cdot \frac{1}{1+e^{-kF_n(t-t_0)(\frac{F_n}{t_0}-1)}} + \dots\right]$ with $k = \frac{2\times 2.92}{t_e - t_s}$ and $t_0 = t_s + \frac{1}{2}(t_e - t_s)$ with t_s start and t_e end time of transients

Capital letters (*A,B, F*) stand for the model parameters, for example the magnitude of the linear component A_2.

conclusion, we do not need to consider the east-west component for this study.

III. RESULTS

A. Ground Motion Analyzer

Fig. 3 shows the results of the GMA for Frankfurt Fig. 3(a) and (c) and Crumstadt Fig. 3(b) and (d), South Hesse, Germany. Areas within the error range are completely filtered out. Although there is a loss of resolution in some areas, regions with particularly strong ground movements are highlighted. In particular, areas that are otherwise framed by low velocities are clearly visible. This helps to concentrate more quickly on regions with significantly higher ground movement in the observation area and time period. In this case, the inner city area of Frankfurt is particularly interesting, as several high-rise buildings and critical infrastructure are located here [blue area in Fig. 3(a)].

The area extending from SW to NE in the left part of the map is the Höchst industrial area, which is also affected by strong subsidence. Other areas include the Dreieich landfill site in the southeast of the map, north of Langen (Hesse), which has a solar park on top that has excellent PSs (east of the small lake at the southern boundary of the map), and several smaller locations along the railways on the southern banks of the Main river, the latter crosses the map diagonally from SW to NE. While the subsidence of the Dreieich landfill can be explained by the compaction of the waste, the cause of subsidence along the railroad tracks on the south bank of the Main cannot be clearly identified. The same applies to the large area in the Höchst area, which is most likely caused by groundwater subsidence based on previous large scale groundwater extraction from industry factories. However, at the time of this study, we did not have any groundwater level measurement data in this area.

No ground movements can be detected for Crumstadt [Fig. 3(d)]. This is partly due to the low average velocity and the relatively strong fluctuations over the course of the year. Only in Hahn, near the already known building damages, does the GMA report increased values. This region was therefore selected anyway. Other criteria were the somewhat more rural surroundings and the proximity to the gas storage facility, which is the subject of current research.

B. Case Study: Frankfurt City

The inner city of Frankfurt a.M. has been identified as a region of strong ground motion by the GMA Fig. 3(c). Several regions in the urban area of Frankfurt show anomalies in ground movement (Fig. 4). Parts of the city are subsiding and others show uplift. While the outer subsidence area is detected with the GMA, the inner subsidence has a too high covariance and is filtered out. Similarly, the uplift area has a too small magnitude to be detected.

On average the inner city shows a stable ground motion with increasing variance starting in the second half of 2018 Fig. 4(a). The inverted linear component for this region shows a very slow subsidence rate of -0.43 $\frac{mm}{a}$ and no regular annual variation (Table II). The weak subsidence trend can be explained by the fact that the strongly subsiding areas are located within the area and therefore influence the average movement rate. Outside the areas of strong subsidence, the average movement is zero.

One of these areas is located around the “Europaviertel” in the western region of the city [Fig. 4(b) and (c)]. This region is further subdivided into an outer region of weak subsidence and an inner region of strong subsidence. Another smaller region of uplift is concentrated along the train tracks toward the east in the southeastern corner of the area of interest which we did not consider here. In general, the subsidence rate in these areas is -1.27 $\frac{mm}{a}$ which more than doubles to -2.91 $\frac{mm}{a}$ in the central area, where several new buildings and an underground metro station have been constructed over the last ten years. A closer

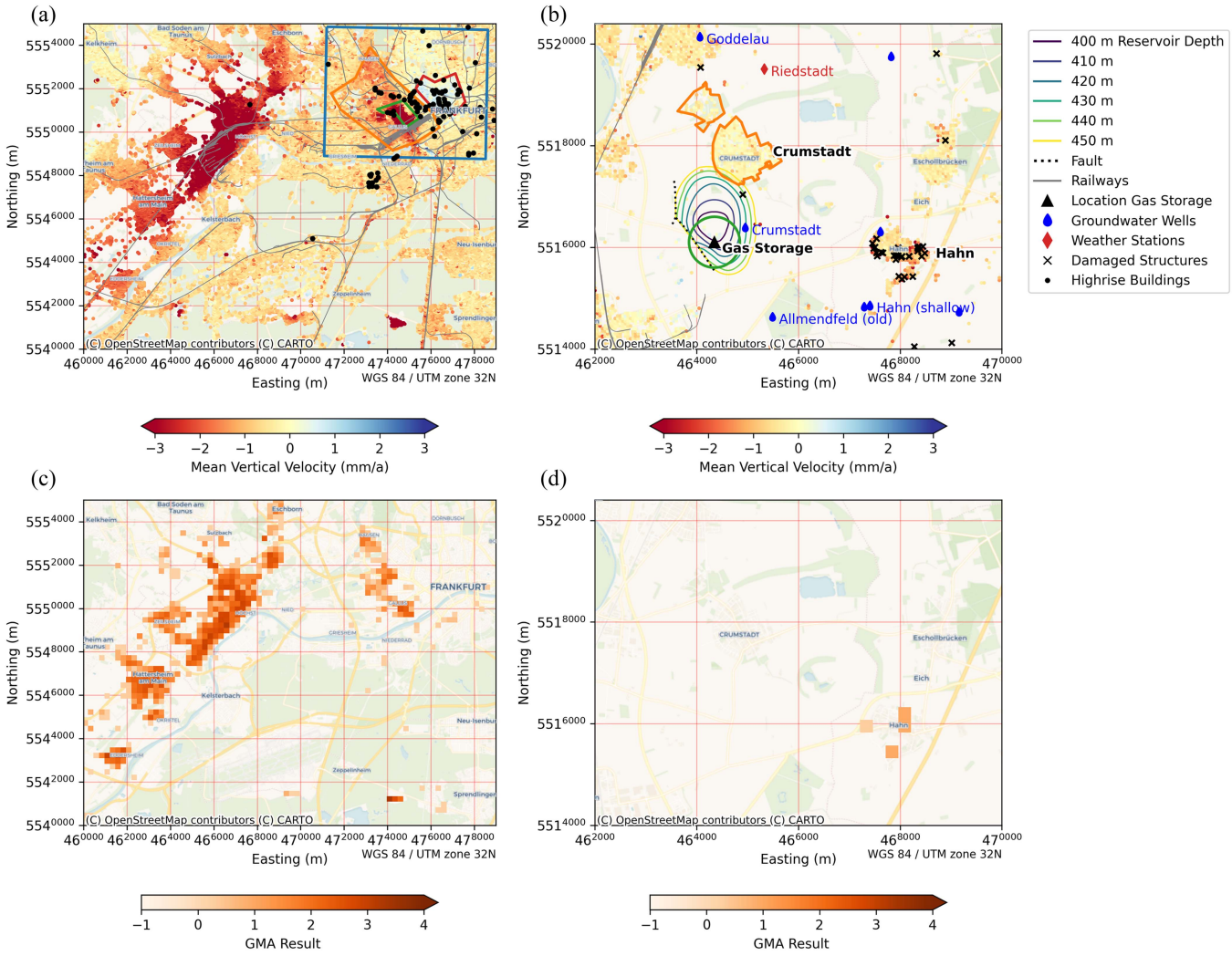

Fig. 3. (a) and (b): Visualization of PSI Data in (a) Frankfurt am Main and (b) Crumstadt. The legend on the right applies to both maps. Please note that the groundwater wells are not shown in (a) because they are too many. The color coded polygons (blue, orange, green and red) correspond to the colors of the inversion plots in Fig. 4(a)–(d) and Fig. 5(a) and (b). (c) and (d): Results for the GMA in (c) Frankfurt am Main and (d) Crumstadt. The filter parameters are: cell size 250 m, minimum vertical velocity $\pm 1.5\ \frac{mm}{a}$ and covariance $\sigma^2 < 1$.

TABLE II
INVERSION RESULTS FOR THE REGIONS IN FRANKFURT A.M. (FIG. 4) AND CRUMSTADT [FIG. 5(A)+(B)]

Parameter	Inner City	Outer Sub.	Inner Sub.	Uplift	Crumstadt	Gas Storage (500 m radius)
linear trend $(\frac{mm}{a})$	-0.43	-1.27	-2.91	0.22	-0.09	0.58
annual sin (mm)	0.00	-0.04	-0.30	-0.21	-2.53	-6.50
annual cos (mm)	-0.03	-0.03	-0.17	0.15	0.92	0.54
max. annual (mm)	0.03	0.05	0.35	0.25	2.69	6.52
annual peak time	30.06.	25.08.	01.09.	06.11.	21.10.	06.10.
semiann. sin (mm)	-0.03	-0.03	0.03	-0.05	-0.01	-0.17
semiann. cos (mm)	-0.02	-0.03	0.01	-0.06	-0.04	0.02
max. semiann. (mm)	0.03	0.04	0.03	0.08	0.04	0.17
semiann. peak time	30.04.	26.04.	03.02.	21.04.	07.04.	22.05
transient no. 1 (mm)	-	-	8.90	-3.57	-	-
transient no. 2 (mm)	-	-	-4.8	1.9	-	-

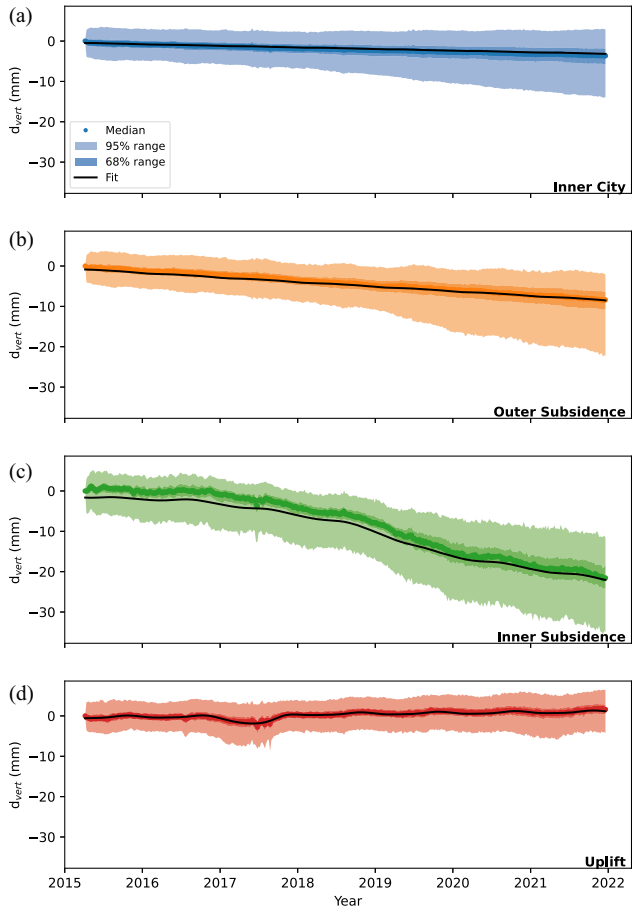

Fig. 4. Time series of vertical movement of selected areas in the city of Frankfurt a.M., Germany. The color code is the same as for the polygons in Fig. 3(a). The legend in a) applies to all plots. The ranges (68 and 95%) correspond to approximately 1 and 2 standard deviations of the data distribution, but better show the sometimes strong nonnormal distribution than the standard deviation of all values at a certain point in time. a) Time series for the whole area with stable average vertical ground motion. The fit results are shown in Table II. b) Time series for the area that shows an overall subsiding trend. c) Time series of the region around the "Europaviertel". The arrows indicate phases with proposed transient movements and their magnitude. d) Time series of the region that shows a weak uplift north of the city center.

look at the time series of the inner subsidence area reveals that from the mid of 2018 onward, the subsidence rate is especially high [Fig. 4(c)]. Therefore we fit a transient subsidence event between these points in time which yields an additional subsidence of -4.8 mm. This transient is also the main reason for the increase of variance in the time series of the whole region after 2018 [Fig. 4(b)]. Closer inspection of the residuals also revealed that between 2015 and 2017 a period of transient uplift of +8.9 mm is needed to explain the time series curve. Besides the linear trend, the inner subsidence region shows higher than average seasonal motion of $\pm$0.35 mm with a peak in the beginning of May.

The area north of Frankfurt central station, namely, between "Bahnhofsviertel" and "Westend," shows an overall uplift [Fig. 4(d)]. The linear component of uplift of +0.22 $\frac{mm}{a}$ is smaller than the general subsidence of the area of interest and therefore not detected by the GMA. The seasonal variation is higher than average but slightly smaller than for the inner subsidence region with a maximum amplitude of $\pm$0.25 mm and a peak in November which is later than for the inner subsidence. In addition, there is a short period of subsidence, followed by uplift between late 2016 and end of 2017. The transient event has an almost double amount of subsidence (-3.57 mm) than the subsequent uplift (+1.9 mm).

For all regions the semiannual component is very small and close to the error margin of the fit. Interestingly, the peak times of the semiannual motion are mostly in late April (or late October, respectively) for all datasets. However, due to the small contribution to the overall signal we ignore the semiannual components for our analysis.

C. Case Study: Crumstadt

The village of Crumstadt, which is located approximately 35 km southwest of Frankfurt, was identified as a region with particularly strong seasonal ground movement [Fig. 5(a)]. The linear components in the Crumstadt region are neutral (-0.09 $\frac{mm}{a}$ in Crumstadt, Table II) to slightly uplifting (0.58 $\frac{mm}{a}$ at Gas Storage, Table II). What is unusual here is the particularly strong annual variation of $\pm$2.7 to 6.5 mm with a maximum in October. As in Frankfurt, the semiannual components are not significant. Due to the location in the floodplain area of the Rhine and the old Neckar, as well as the immediate proximity of a gas reservoir to the village, it is likely that one of these factors explains the strong annual fluctuations. Such strong fluctuations cannot be observed anywhere else in southern Hesse, especially over an area of several square kilometers. We therefore examined various external data sources.

To investigate this in more detail, a time series analysis of the PSs in the residential area and in the area of maximum seasonality near an underground gas storage facility is carried out [Fig. 5(a) and (b)]. In addition to the ground movement, further data are included in the analysis. Precipitation data and temperature data are taken from the nearest weather station of the German Weather Service (DWD) in Frankfurt and others close-by [Fig. 5(c) and (e)]. Groundwater levels are determined from three permanent groundwater measuring points in the vicinity of the area under investigation [Fig. 5(e)]. Furthermore, the filling levels of the gas storage facility were obtained from the operator's website [Fig. 5(f)].

Various trends emerge when analyzing external data. First, the precipitation data [Fig. 5(c)] are of low resolution and therefore not very suitable for this analysis. Furthermore, no clear seasonality can be identified in the observation period. Although there tends to be heavy precipitation in the summer months, this is not particularly clear in some years (especially 2015, 2018, and 2020). The temperature data [Fig. 5(d)] are fairly consistent over a large area. The measuring stations are located between 1.6 km (Riedstadt) and a maximum of 23 km (Raunheim) away. The average annual fluctuation is approx. 9.3° C and shows a maximum in mid-July. The groundwater measurements [Fig. 5(e)] show hardly any seasonal effects, similar to the precipitation data. A weak connection can be drawn between heavy precipitation in spring 2016 and an increase in

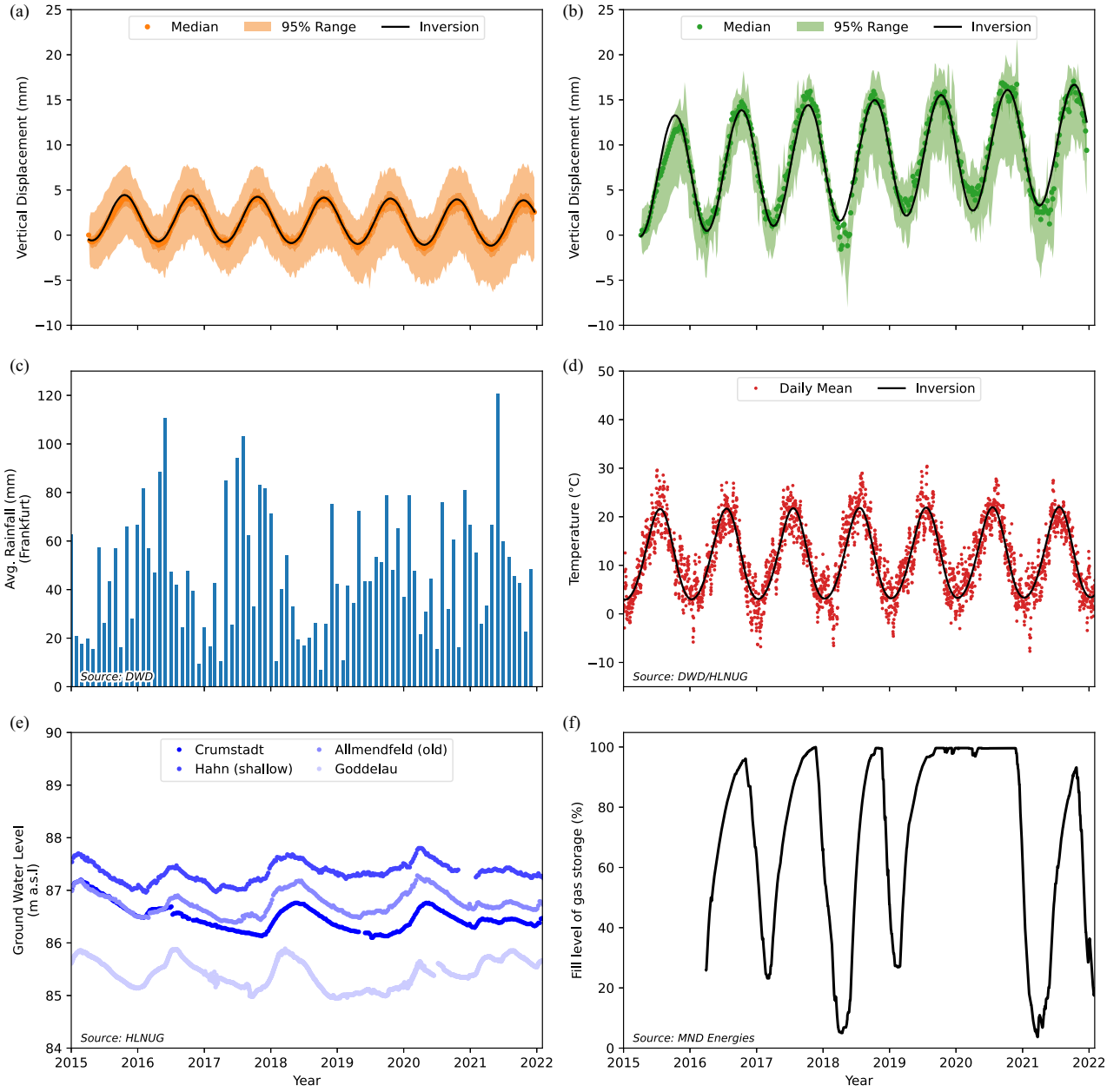

Fig. 5. Time series data and external datasets from specific sites in the Crumstadt area. The color code is equal to the polygons and symbols in Fig. 3(b). (a) Time series of the vertical displacement of PSs in Crumstadt. (b) Time series of the vertical displacement of PSs in a 500-m radius around the gas storage site. (c) Average precipitation of the nearest weather station with a rain gauge whose readings were available (lies outside of the map section). (d) Average daily temperature in the study area, calculated from the values of the four nearest stations. Only the Riedstadt weather station is included in the map section, the other three (Darmstadt, Mörfelden and Raunheim) lie outside. (e) Ground water level at four monitoring stations close to the gas storage. (f) Fill level of the gas storage as percentage of recorded maximum fill level.

the groundwater level. In dry years, a tendency toward a decrease can be observed, interrupted by two strong increases in the first halves of 2018 and 2020. These trends can be seen in all four stations, so they are probably hydraulically connected through the ancient river bed of the Neckar river (fell dry in the 1st century AD). Only the "Goddelau" station reached the maximum level earlier in 2018 and 2020 than the other stations. This could be due to its proximity to an almost abandoned meander of the river Rhine (visible at the northwestern corner of the map in Fig. 3(b), called "Kühkopf-Knoblochsaue"). The filling level of the gas storage facility fluctuates considerably over the course of the year. However, there are years in which the storage facility either reaches particularly low filling levels, such as in 2018 and 2021, or remains at a constantly high level, such as in 2020. The filling rates also vary in the different years, but are generally somewhat lower than the withdrawal rates. Filling takes place quickly at the beginning and decreases slowly toward the end. In contrast, withdrawal starts immediately at a roughly linear rate and remains constant until the minimum level is reached.

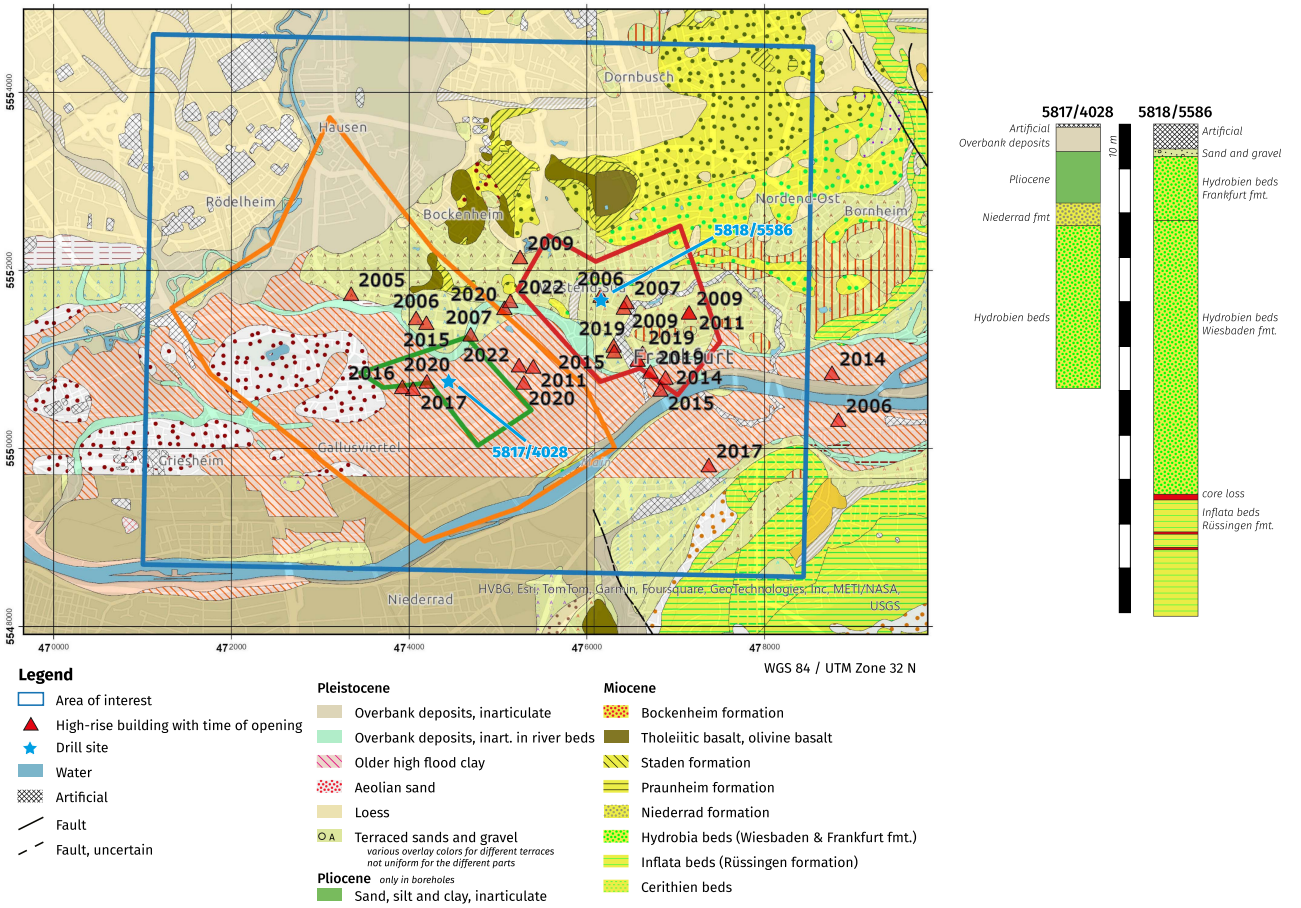

Fig. 6. Geological map of the study area in Frankfurt a.M. and drill logs from the "Inner subsidence" and "Uplift" region. This map only shows high-rise buildings that were opened no more than ten years before the PSI data was collected. Map is based on the geological map of Hessen (1:25000, [29]) and the legend includes only the most important lithologies. The drill logs are derived from the drill log database by HLNUG (C. Hoselmann, pers. comm.).

IV. Discussion

A. Limitations of the Time Series Analysis

In its current state the time series analysis that we used in this study has several important limitations. The main source of uncertainty is the manual definition of the transient periods. Up to now, this has been done by manually checking the fit residuals and can produce different results depending on the specified start and end times. The number of transients required is another factor. For example, to reduce the error in the time series for the inner subsidence [Fig. 4(d)], a fairly high uplift is required, which must start before the measurements begin. This can only be seen here from the fits and cannot be verified by additional measurements from the same campaign. A link with data from previous missions (e.g., ERS-2) would be possible, but these have a completely different resolution and have not been available to us so far. Another possibility might be to implement an iterative scheme to search for transients using a segmentation algorithm, e.g., as used by [33].

In some cases, it is also not clear whether the transient functions interact with the sinusoidal components, which in the case of Fig. 4(e) leads to stronger subsidence compared to the uplift. In a qualitative view, the value approaches the general trend again, so an equal uplift magnitude would be more likely than the currently determined value. However, if a transient uplift coincides exactly with the seasonal increase, this could influence the measured amount.

B. Classification of Causes of Ground Motion in Frankfurt a.M.

The zone with the highest subsidence rates is in the "Europaviertel" area, which is a new inner city quarter in Frankfurt. Construction work began in 2005 and is largely located in the area of the former goods station, a large open space without high-rise buildings (Fig. 6). The new buildings are mostly multistorey apartment blocks and individual high-rise buildings. These can cause several types of ground movement.

The most probable cause of subsidence in the area of the "Europaviertel" is the extraction of groundwater as part of the dewatering of the deep construction pits. For example, the groundwater table is less than 10 m deep [34], with foundation depths of over 35 m often required, and even up to 50 m at the construction site of the subway station. A lowering of several tens of meters is therefore often necessary. The time periods involved here amount to a few years in which the groundwater in a particular area is kept at a long-term low level. As can be seen in Fig. 6, the most recently opened high-rise buildings

are located within or near the "inner subsidence" (green). This coincidence in time fits very well with the increased downward movement from around 2017 [Fig. 4(c)].

The main geological units in this region are quaternary unconsolidated sediments, and various tertiary layers of mudstone, marls, and sands, sometimes interbedded with limestones [29], [35]. All these units form a complex sequence of aquifers and aquitards which carry different amounts of groundwater. With the main aquifers being the quaternary sediments and sandy layers of the upper "Hydrobien" beds. In addition, the limestone layers are also known to act as fracture and karst aquifers in nearby regions. The muds, silty sands, and clay layers act as aquitards and dissect the aquifers into several layers. The limestone beds and unconsolidated quaternary sediments can cause large amounts of ground water influx into the construction sites and therefore water is usually produced from these formations in order to lower the ground water level.

Previous studies have shown that due to ground water extraction and the additional load of high rise buildings a short-term (month to year) subsidence of up to 25 mm and a long-term subsidence of up to 250 mm can be expected in this area [15]. In addition to the load, the change in the subsoil due to the introduction of soil-improving bulk materials in the foundation area also plays a role, although the subsequent compaction should be small due to suitable compaction measures. Furthermore, during construction the removal of material leads to an extended zone of deformation surrounding the building pit [36]. Due to the geological conditions in Frankfurt, this is particularly pronounced in the urban area and makes additional measures necessary.

The affected area of subsidence extends much farther north than the immediate surroundings of the construction sites. The main aquifer in the study region belongs to the so-called "Wetterau" region, consists of Pliocene gravels and sands, and has a medium hydraulic conductivity (10^{-4} to 10^{-3} $\frac{m}{s}$ [37]). We estimate that the prevailing ground water flow is directed toward the Main river, based on the groundwater map by [34] which covers the region southeast of the study area. The Pliocene sands can only be detected in the area of the subsidence (borehole 5817/4028, Fig. 6) and are no longer present in the eastern part of the city (borehole 5818/5586, Fig. 6). This could explain the different uplift and subsidence directions between the areas as well as the NW-SE elongated shape. The Pliocene sediments and overbank deposits above the "Hydrobien" beds are known to include clay layers that were classified as prone to shrink and swell by the local authorities. They thin out toward the east and are very thin to absent in the area of uplift.

The uplift in the region north of the old town might be caused by swelling of the mudstones or expansion of pore space in sandy layers due to groundwater influx. Construction of high-rise buildings is prevalent in the area since the late 1960 s. In the area of highest uplift, no high-rise buildings have been constructed since the late 2000 s. A natural balance of groundwater recharge and groundwater discharge is likely to be restored there. It is also possible that the location at the edge of the aquifer plays a role. The unconsolidated quaternary sediments are mostly absent and the tertiary formations are slightly older. Here, muds and silty marls from the lower "Hydrobien" Beds and the Rüssingen formation are located at a higher level than in the subsidence region (Fig. 6). These have lower permeability coefficients (10^{-7} to 10^{-5} $\frac{m}{s}$ [37]) and represent an aquitard, so that the regions are most likely not hydraulically connected.

The transient period during 2017 is most dominant in the southwestern corner of the uplift region, where several old high-rise buildings were demolished and new ones were built, with several still being under construction (ages of buildings in Fig. 6). As most of the projects have already been completed or are scheduled for completion in 2024, it is very likely that the phase with deep construction pits has already been completed. This means that only a low level of subsidence can be measured in this region at the end of the 2021 monitoring period. In contrast, the "Europaviertel" region still has a deep underground construction pit, which means that groundwater still has to be pumped out there.

C. *Classification of Causes of Ground Motion in Crumstadt*

The strong seasonal fluctuations in Crumstadt must be caused by a process with similar periodicity. The primary factor with a similar periodicity, which was also present in our database, is temperature. However, the maximum of the average temperature is in mid-July, whereas the maximum elevation is reached in October, a difference of almost three months (Table II). A time series correlation of the data with seasonality and linear trend with the temperature data also shows a correlation of 95 days for Crumstadt [Fig. 7(a)] and 77 days for the gas storage site [Fig. 7(b)]. It should be noted here that the signals have a strong autocorrelation and therefore the cross-correlation only works to a limited extent. To calculate the cross-correlation, the temperature and gas storage time series were downsampled to the same interval as the PSI data (from daily to six-day intervals) and then cross correlated using a sum-based convolution. Another factor is the filling level of the gas storage facility, which reaches its maximum around October, but is not as regular as the temperature fluctuation. At first glance, neither precipitation nor groundwater levels appear to correlate with soil movements. It may be possible to identify a link by analyzing both time series in detail using a different methodology, for example, as in [33]. In its current form, the inversion algorithm is not able to process time series with irregular or multiyear cycles. It must therefore be adapted for future studies.

In addition to the temporal variation, there should be a feature near Crumstadt that makes this area special, as the fluctuations do not occur outside this region. The gas storage facility is also a good option here. In particular, the increase in seasonality from NE to SW, in the direction of the storage facility, suggests a link between filling level and soil movement. The lack of ground movement in the west, e.g., in Stockstadt, can be explained by two faults [Fig. 3(b)]. These run in an N–S direction to the west of the reservoir and could act as a tectonic and hydraulic barrier to the movement in the reservoir. In addition to the "Stockstadt" storage facility, there is another storage facility to the southeast of the investigated region near Hähnlein. There

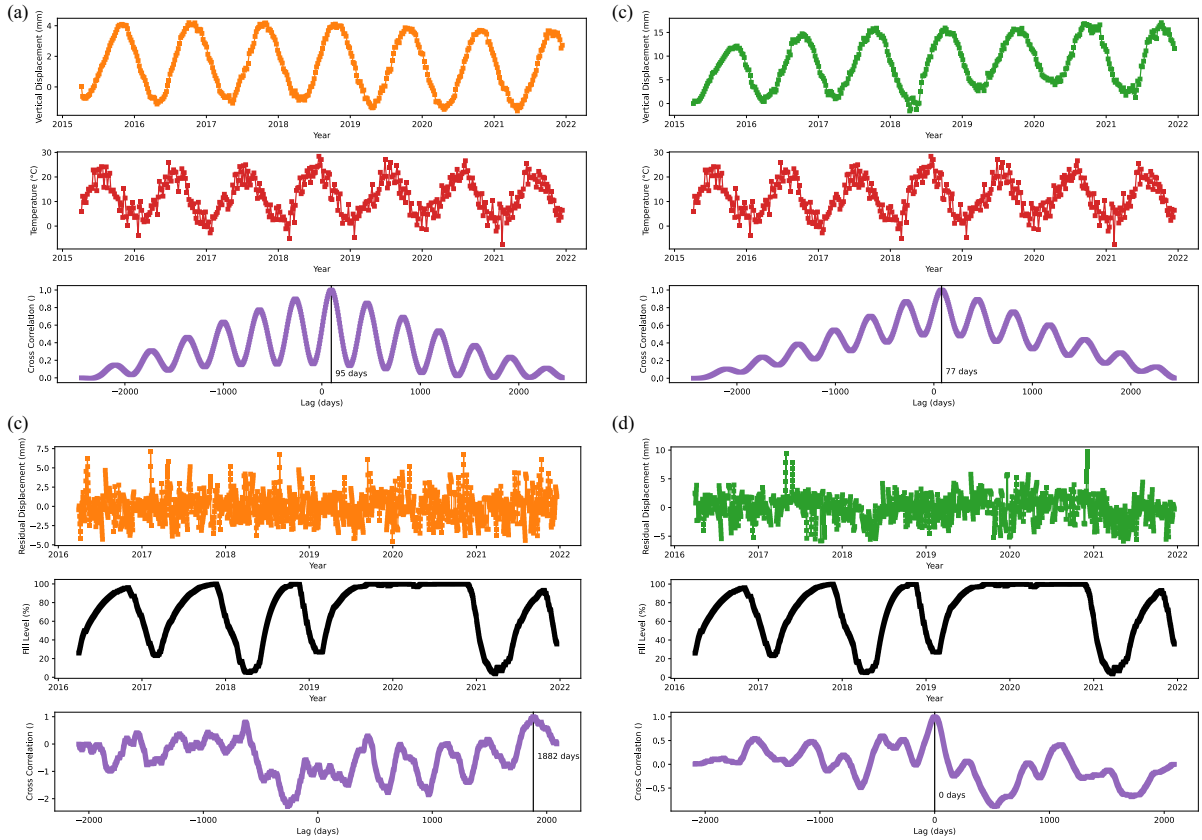

Fig. 7. Cross-correlation diagrams of some signals with the average PS motion. The color scheme follows the same as in Fig. 5. (a) Ground motion in Crumstadt versus temperature. (b) Ground motion atop gas storage versus temperature. (c) Residual ground motion in Crumstadt versus gas storage fill level. (d) Residual ground motion atop gas storage versus gas storage fill level.

are no fluctuations in Hähnlein that are greater than normal. One reason might be that this reservoir has a different filling pattern. Another reason could be that although the reservoir is in the same geological unit, it is found about 100 m deeper due to normal faulting and the resulting compartimentalization of the reservoir.

Since we assume that the main part of the movements is determined by the seasonal and linear component, we also try to quantify a link to the gas storage level with the help of cross-correlation. For this purpose, we use the residuals of the time series analysis and correlate them with the filling level of the gas storage facility. No correlation can be established for Crumstadt [Fig. 7(c)]. For the measured values directly above the gas storage facility, the correlation is highest with a lag of zero days [Fig. 7(d)]. An instantaneous reaction of the soil movements to the filling level can be interpreted by elastic deformation of the rock units to increase the pressure in the reservoir. This correlation can also be recognized qualitatively. For example, in years when the filling level reaches minimum values (2018 and 2021), a few mm greater subsidence can also be measured. A fill level of 20% may be a threshold value here. In contrast, in 2020, where no extraction took place, a less pronounced subsidence of the surface can be measured. Overall, the filling level of the gas storage reservoir therefore appears to have an average influence of around ± 2 mm. However, entire filling or extraction cycles cannot be derived directly from the ground movements measured by the PSI data of the BBD. Comparing our dataset with the EGMS we find that the data in the EGMS shows a better correlation with the filling level of the reservoir. This is probably due to the differences in PS-InSAR processing between the BBD and EGMS datasets. Thus, the use of EGMS data seems more suitable for such analyses.

The entire region is characterized by old meanders of the Rhine and Neckar rivers. The latter flowed in this region until around 2000 years ago. The semicircular shape of Crumstadt follows a former branch of the Neckar, which is also located above the "Hähnlein" gas reservoir. So at least the soil conditions in the uppermost meters seem to have little influence. However, these consist of materials that are particularly prone to swelling. In the central area of the oxbow lakes it is mainly peat and in the other areas mainly clayey sediments that can swell. The moisture in the uppermost soil layers is also largely influenced by the temperature, so it may well be that the topsoil dries out and shrinks in particularly warm seasons with little precipitation. This movement is contrary to the general trend of uplift which has a peak in summer.

Groundwater fluctuations are often cited as a possible cause. In this case, however, it is not possible to bring the fluctuation of the groundwater level into temporal harmony with the ground movements. Particularly as the soil conditions and groundwater levels are similar throughout the region, the fluctuations should also occur in the neighboring regions. A local groundwater

anomaly due to the activity in the gas reservoir can also be ruled out, as the nearest station is only 600 m away from the reservoir.

V. Conclusion

In this article, we used the GMA to analyze PSI data for the whole state of Hesse, Germany. It filters PS based on variance and number criteria, allowing visualization of regions with strong ground movement at different spatial scales. In two case studies, one in Frankfurt and another in Crumstadt we found patterns that significantly differ from the average in the state. The causes of ground motion in Frankfurt include construction-related groundwater extraction, while in Crumstadt, seasonal fluctuations are associated with temperature variations and the filling level of a gas storage facility. The impact of local geological conditions is also discussed. In both cases, it is not possible to conclusively determine the exact cause of the respective anomalies. Either relevant data are missing or the respective reasons were not sufficiently taken into account in the time series analysis. Due to the limitations in the time series analysis, such as the manual definition of transient periods and the challenge of processing irregular or multiyear cycles we suggest further improvements and adaptations in future studies.

In this study, we show the applicability of ground motion service data to engineering geology issues. In particular, the long-term monitoring of construction activities or the use of the subsurface can be more easily monitored by the relevant authorities using our workflow. For example, it can be determined whether there are still measurable subsidence phenomena in an area due to construction activities and whether these could possibly cause damage to buildings (e.g., in Frankfurt). Or it would be possible to quantify the respective proportions of seasonal fluctuations and reservoir levels more precisely (e.g., for the Stockstadt/Crumstadt gas storage). This improves the estimation of the rock parameters in the reservoir area and can be used for more accurate geomechanical models of the reservoir and its use as underground gas storage. Our methodology is an addition to existing ground-based surveying methods and can also be used to detect previously unknown movements in urban areas. For example, it was not previously known that there were significantly increased ground movements in the vicinity of the gas storage facility close to Crumstadt.

Our results emphasize the importance of comprehensive ground motion analysis for effective urban planning, risk assessment, and understanding the impact of anthropogenic activities and climate-induced changes on subsurface dynamics. Not only the average surface movement over several years should be considered but also the different components of a time series analysis. In this way, regular or transient movements can also be adequately described. For a comprehensive analysis of ground movements, the integration of external data, such as temperature, precipitation, and various other data above and below the surface is required.

Acknowledgment

The authors would like to thank the other departments of the Hessian Agency for Nature Conservation, Environment and Geology, which gave access to their data, in particular B. Oehme, N. Poppendick, S. Schäfer. C. Dorn from the Hessian State Office for Soil Management and Geoinformation is thanked for his assistance in analyzing the spatial data. The authors would also like to thank S. Metzger from Helmholtz Centre Potsdam for providing the source code of their inversion algorithm.

References

[1] T. Dijkstra and N. Dixon, "Climate change and slope stability in the U.K.: Challenges and approaches," *Quart. J. Eng. Geol. Hydrogeol.*, vol. 43, no. 4, pp. 371–385, Nov. 2010.

[2] S. L. Gariano and F. Guzzetti, "Landslides in a changing climate," *Earth-Sci. Rev.*, vol. 162, pp. 227–252, Nov. 2016.

[3] A. Barra et al., "From satellite interferometry displacements to potential damage maps: A tool for risk reduction and urban planning," *Remote Sens. Environ.*, vol. 282, Dec. 2022, Art. no. 113294.

[4] A. K. Gabriel, R. M. Goldstein, and H. A. Zebker, "Mapping small elevation changes over large areas: Differential radar interferometry," *J. Geophysical Res.*, vol. 94, no. B7, 1989, Art. no. 9183.

[5] D. Massonnet et al., "The displacement field of the landers earthquake mapped by radar interferometry," *Nature*, vol. 364, no. 6433, pp. 138–142, 1993.

[6] A. Ferretti, C. Prati, and F. Rocca, "Permanent scatterers in SAR interferometry," *IEEE Trans. Geosci. Remote Sens.*, vol. 39, no. 1, pp. 8–20, Jan. 2001.

[7] M. Motagh et al., "Quantifying groundwater exploitation induced subsidence in the Rafsanjan plain, Southeastern Iran, using InSAR time-series and in situ measurements," *Eng. Geol.*, vol. 218, pp. 134–151, Feb. 2017.

[8] P.-Y. Declercq, P. Gerard, E. Pirard, D. Perissin, J. Walstra, and X. Devleeschouwer, "Subsidence related to groundwater pumping for breweries in Merchtem area (Belgium), highlighted by persistent scaterrer interferometry," *Int. J. Appl. Earth Observ. Geoinformation*, vol. 63, pp. 178–185, Dec. 2017.

[9] M. A. Hussain et al., "PS-InSAR based monitoring of land subsidence by groundwater extraction for Lahore metropolitan city, Pakistan," *Remote Sens.*, vol. 14, no. 16, Aug. 2022, Art. no. 3950.

[10] J. Liu, F. Ma, G. Li, J. Guo, Y. Wan, and Y. Song, "Evolution assessment of mining subsidence characteristics using SBAS and PS interferometry in Sanshandao gold mine, China," *Remote Sens.*, vol. 14, no. 2, Jan. 2022, Art. no. 290.

[11] M. Przylucka, Z. Kowalski, and Z. Perski, "Twenty years of coal mining-induced subsidence in the Upper Silesia in Poland identified using InSAR," *Int. J. Coal Sci. Technol.*, vol. 9, no. 1, Nov. 2022, Art. no. 86.

[12] L. Bateson, F. Cigna, D. Boon, and A. Sowter, "The application of the intermittent SBAS (ISBAS) InSAR method to the South Wales coalfield, U.K," *Int. J. Appl. Earth Observ. Geoinformation*, vol. 34, pp. 249–257, Feb. 2015.

[13] P. Gonnuru and S. Kumar, "PsInSAR based land subsidence estimation of Burgan oil field using TerraSAR-X data," *Remote Sens. Appl.: Soc. Environ.*, vol. 9, pp. 17–25, Jan. 2018.

[14] J. D. Smith, J. Avouac, R. S. White, A. Copley, A. Gualandi, and S. Bourne, "Reconciling the long-term relationship between reservoir pore pressure depletion and compaction in the Groningen Region," *J. Geophysical Res.: Solid Earth*, vol. 124, no. 6, pp. 6165–6178, Jun. 2019.

[15] D. Peduto, M. Santoro, M. Graziuso, M. Korff, and H. van Meerten, "Combined subsidence phenomena in high-rise built urban areas: Numerical study for frankfurt am main," in *Proc. XVII Eur. Conf. Soil Mechanics Geotechnical Eng.*, 2019, pp. 1966–1973.

[16] Z. Zhang, C. Hu, Z. Wu, Z. Zhang, S. Yang, and W. Yang, "Monitoring and analysis of ground subsidence in Shanghai based on PS-InSAR and SBAS-InSAR technologies," *Sci. Rep.*, vol. 13, no. 1, May 2023, Art. no. 8031.

[17] M. Gao et al., "InSAR time-series investigation of long-term ground displacement at Beijing Capital International Airport China," *Tectonophysics*, vol. 691, pp. 271–281, Nov. 2016.

[18] A. Kalia, "User driven products in the context of the ground motion service Germany," in *Proc. IEEE Int. Geosci. Remote Sens. Symp.*, 2017, pp. 1688–1691.

[19] R. Czikhardt, J. Papco, M. Bakon, P. Liscak, P. Ondrejka, and M. Zlocha, "Ground stability monitoring of undermined and landslide prone areas by means of Sentinel-1 multi-temporal InSAR, case study from Slovakia," *Geosciences*, vol. 7, no. 3, Sep. 2017, Art. no. 87.

[20] A. Kalia, "Classification of landslide activity on a regional scale using persistent scatterer interferometry at the Moselle valley (Germany)," *Remote Sens.*, vol. 10, no. 12, Nov. 2018, Art. no. 1880.
[21] K. Krzepek, M. Rudolf, B. Homuth, A. Henk, and D. Iwaszczuk, "Raster representation of ground motion service data and automated hot-spot detection," in *Proc. IEEE Joint Urban Remote Sens. Event*, 2023, pp. 1–4.
[22] A. Barra et al., "A methodology to detect and update active deformation areas based on sentinel-1 SAR images," *Remote Sens.*, vol. 9, no. 10, Sep. 2017, Art. no. 1002.
[23] Pagán Tomás et al., "Semi-automatic identification and pre-screening of geological–geotechnical deformational processes using persistent scatterer interferometry datasets," *Remote Sens.*, vol. 11, no. 14, Jul. 2019, Art. no. 1675.
[24] J. A. Navarro et al., "Adatools: Automatic detection and classification of active deformation areas from PSI displacement maps," *ISPRS Int. J. Geo-Inf.*, vol. 9, no. 10, Oct. 2020, Art. no. 584.
[25] J. Cohen-Waeber, R. Bürgmann, E. Chaussard, C. Giannico, and A. Ferretti, "Spatiotemporal patterns of precipitation–modulated landslide deformation from independent component analysis of InSAR time series," *Geophysical Res. Lett.*, vol. 45, no. 4, pp. 1878–1887, 2018.
[26] M. H. Haghighi and M. Motagh, "Assessment of ground surface displacement in Taihape landslide, New Zealand, with C- and X-band SAR interferometry," *New Zealand J. Geol. Geophys.*, vol. 59, no. 1, pp. 136–146, 2016.
[27] R. Tomás, Z. Li, J. M. Lopez-Sanchez, P. Liu, and A. Singleton, "Using wavelet tools to analyse seasonal variations from InSAR time-series data: A case study of the Huangtupo landslide," *Landslides*, vol. 13, no. 3, pp. 437–450, 2016.
[28] Y. Liu et al., "Deformation responses of landslides to seasonal rainfall based on InSAR and wavelet analysis," *Landslides*, vol. 19, no. 1, pp. 199–210, 2022.
[29] HLNUG, Wiesbaden, Germany, Geologische karten von hessen 1:25000. hessisches landesamt für naturschutz, umwelt und geologie, 2017. [Online]. Available: https://www.geoportal.hessen.de/spatial-objects/268
[30] A. Kalia, M. Frei, and T. Lege, "BodenBewegungsdienst Deutschland (BBD): Konzept, umsetzung und service-plattform," *Zfv*, vol. 146, pp. 273–279, 2021.
[31] S. Metzger et al., "Present kinematics of the Tjörnes fracture zone, North Iceland, from campaign and continuous GPS measurements," *Geophysical J. Int.*, vol. 192, no. 2, pp. 441–455, Nov. 2012.
[32] M. Bevis and A. Brown, "Trajectory models and reference frames for crustal motion geodesy," *J. Geodesy*, vol. 88, no. 3, pp. 283–311, Jan. 2014.
[33] M. Evers, A. Thiele, H. Hammer, and S. Hinz, "PSDefoPAT-persistent scatterer deformation pattern analysis tool," *Remote Sens.*, vol. 15, no. 19, Sep. 2023, Art. no. 4646.
[34] HLNUG, Wiesbaden, Germany, "Grundwasserflurabstand im Oktober 2015 Hydrologisches Kartenwerk," 2016. [Online]. Available: https://www.hlnug.de/fileadmin/img_content/wasser/grundwasser/grundwasserkarten/ried_15_okt_fl.pdf
[35] R. Becker and T. Reischmann, *Geologie Von Hessen*. Stuttgart, Germany: Schweizerbart'sche Verlagsbuchhandlung, 2021.
[36] C. Moormann, "Analysis of wall and ground movements due to deep excavations in soft soil based on a new worldwide database," *Soils Foundations*, vol. 44, no. 1, pp. 87–98, Feb. 2004.
[37] BGR, Berlin, Germany, "Hydrogeologische Übersichtskarte 1:250.000 von Deutschland (HÜK250)," Mar. 2019. [Online]. Available: https://services.bgr.de/grundwasser/huek250

Michael Rudolf received the master's degree in geology from the Albert-Ludwigs-University Freiburg, Freiburg im Breisgau, Germany, in 2014 and the Ph.D. degree in geology from Free University Berlin, Berlin, Germany, in 2019.

Since 2021, he has been a Staff Scientist and Lecturer with the Group of Engineering Geology, Technical University Darmstadt. For his doctoral thesis and first Postdoc, he worked on the implementation of various materials and experimental setups to model seismotectonic phenomena along strike-slip fault systems with the Laboratory for Experimental Tectonics, Helmholtz Centre Potsdam GFZ, Potsdam, Germany. His research interests include seismotectonics, and frictional and granular mechanics to data analysis focusing on geohazard applications, such as earthquakes or mass movements.

Katrin Krzepek received the master's degree in environmental engineering in 2021 from the Technical University of Darmstadt, Darmstadt, Germany, where she is currently working toward the Ph.D. degree in remote sensing and image analysis, focusing on the use of synthetic aperture radar data for environmental applications, with the Remote Sensing and Image Analysis Group.

Benjamin Homuth received the master's degree in geosciences, with a main emphasis on geophysics, from Goethe University Frankfurt, Frankfurt, Germany, in 2010, and the Ph.D. degree in seismology, focusing on swarm earthquakes, regional stress field, and seismic hazard analyses, in 2015.

Since October 2015, he has been the Head Scientist of the Hessian Earthquake Centre, Hessian Agency for Nature Conservation, Environment and Geology, Wiesbaden, Germany. His research interests include local earthquake and stress field analyses, and geophysical mapping of the near subsurface to the detection of ground motions by remote sensing, i.e., using persistent scatterer interferometry or LiDAR data.

Andreas Henk received the Diploma in geology from the University of Mainz, Mainz, Germany, and the Ph.D. degree in geology and the Habilitation from the University of Würzburg, Würzburg, Germany, in 1991 and 1997, respectively.

He was appointed as a Professor of applied geology with the University of Freiburg, Freiburg im Breisgau, Germany. Since 2012, he has been the Chair of engineering geology with the Institute of Applied Geosciences, Technical University of Darmstadt, Darmstadt, Germany. His research interests include geomechanical-numerical modeling, and safe and sustainable use of the subsurface.

Dorota Iwaszczuk received the master's degree in geodesy and cartography from the AGH University of Science and Technology, Krakow, Poland, and the Ph.D. degree in photogrammetry and remote sensing, focusing on automatic texturing of 3D building models with aerial thermal imagery.

In 2018, she spent six months at the Ohio State University, Columbus, OH, USA, as a Postdoctoral Researcher working on backpack sensor system for indoor and outdoor mapping. Since March 2019, she has been the Professor with the Technical University of Darmstadt, Darmstadt, Germany, where she leads the Remote Sensing and Image Analysis Group. Her research interests include remote sensing and photogrammetry, including but not limited to sensor data fusion, semantic segmentation, LiDAR data processing, 3D reconstruction, 3D scene analysis, IR-thermography, and crowdsourcing.

Dr. Iwaszczuk is the Vice President of the German Society for Photogrammetry, Remote Sensing and Geoinformation, Co-Chair if ISPRS working group ICWG I/IV: Robotics for Mapping and Machine Intelligence as well as the Associate Editor for *Photogrammetric Engineering & Remote Sensing*.